ELSEVIER

Journal of Molecular Catalysis A: Chemical 119 (1997) 201–212

JOURNAL OF MOLECULAR CATALYSIS A: CHEMICAL

Characterization and activity of hydrotalcite-type catalysts for acetonitrile hydrogenation

F. Medina [a], R. Dutartre [a], D. Tichit [a], B. Coq [a], N.T. Dung [a], P. Salagre [b], J.E. Sueiras [c,*]

[a] *Laboratoire de Materiaux Catalytiques et Catalyse en Chimie Organique, C.N.R.S., U.R.A. 418, 8, Rue Ecole Normale, 34053 Montpellier Cedex 1, France*

[b] *Facultat de Química, Universitat Rovira i Virgili, Pl. Imperial Tarraco, 1, 43005 Tarragona, Spain*

[c] *Escola Tècnica Superior d'Enginyeria, Universitat Rovira i Virgili, Pl. Imperial Tarraco, 1, 43005 Tarragona, Spain*

Abstract

Studies of the preparation and characterization using X-ray diffraction, temperature programmed reduction and decomposition, electron microscopy (TEM-SEM), calorimetric measurements, temperature programmed desorption, nitrogen adsorption and the catalytic behavior of three samples having takovite structure with different Ni/Mg/Al ratios in order to modify the basicity of the solid, have been carried out for the acetonitrile hydrogenation reaction in the gas phase. It has been shown that the chemical composition of the samples significantly modifies their catalytic behaviors. Also, low magnesium contents, which cause an increase on basic properties, result in higher activity and selectivity to primary amine. The catalytic properties were correlated with the accessibility and reducibility of Ni particles, and ethylamine adsorption heats. Thermal stability of the takovite materials and their surface properties are also reported.

Keywords: Nickel catalysts; Takovite catalysts; Acetonitrile hydrogenation

1. Introduction

Amines can be prepared commercially by hydrogenation of nitriles [1]. An example is the hydrogenation of adiponitrile, which is used in the manufacture of Nylon-6,6 [2,3]. First the compound is partially hydrogenated to 6-aminohexanenitrile, and then to 1,6-hexanediamine [1].

The industrial preparation of these primary amines is usually accomplished in the liquid phase at elevated hydrogen pressures and temperatures, in the presence of a heterogeneous transition metal catalyst [4,5].

Raney nickel and Raney cobalt are probably the most frequently used catalysts for the primary amine production [6–10]. Other catalysts based on Rh, Mn and Fe have also been reported [11,12]. Because of the high reactivity of partially hydrogenated reaction intermediates, imines or Schiff bases, a conventional hydrogenation leads to a mixture of primary, secondary, and tertiary amines. An excess of ammonia is found to be essential to suppress secondary and tertiary amine formation, presumably due to the presence of an imine intermedi-

* Corresponding author.

1381-1169/97/$17.00 Copyright © 1997 Elsevier Science B.V. All rights reserved.
PII S1381-1169(96)00484-0

ate [13]. Even under these conditions, the primary amine yield is never complete.

All products of the nitrile hydrogenation (primary, secondary, and tertiary amines) are basic species that will interact more strongly with an acidic than with a basic catalyst. Therefore, it has to be expected that on changing the character of the support from acidic to basic, a change in selectivity could be observed in favor of primary amines. Recently [12,14,15], the modification of the intrinsic acidity of catalysts by the application of alkaline additives has been observed to have a large impact on the selectivity of the resulting catalyst.

On the other hand, hydrotalcite-type anionic clays (LDH) may be useful precursors of catalysts. These catalysts also exhibit good activities in hydrogenation processes and the steam reforming reactions [16–22].

At the same time, strong basic properties with Hammet acidity function H_0 values near 17 were identified on some of the oxides produced by calcination of hydrotalcites [23–25]. The number and strength of basic sites both depend on chemical composition and activation conditions [26]. The synthesis control of the precursor could be of interest in designing hydrotalcite-derived basic catalysts. Actually, the way in which these parameters affect the surface basicity, and in fine the catalytic behavior of the active metallic phase, has been scarcely studied and are not well understood.

The aim of this work is the synthesis and characterization of three hydrotalcite-type precursors with different chemical compositions and their catalytic properties were performed in the hydrogenation of acetonitrile in the gas phase.

2. Experimental

2.1. Catalyst preparation

The three hydrotalcite-type precursors, H1, H2 and H3, were prepared by coprecipitation, at room temperature and at constant pH = 8.0 ± 0.2, using aqueous solutions containing $Mg(NO_3)_2 \times 6H_2O$, $Ni(NO_3)_2 \times 6H_2O$ and $Al(NO_3)_3 \times 9H_2O$ in molar ratios Mg/Ni/Al of 0:3:1, 0.5:1.5:1, 1.6:1.5:1, respectively, with a 1 M NH_4OH titrating solution which was simultaneously added to 0.05, 0.05 and 1 M $(NH_4)_2CO_3$ solutions, respectively (the third sample was prepared with a high excess of $(NH_4)_2CO_3$). The addition was performed drop by drop under vigorous magnetic stirring. After complete precipitation the gel was treated for 2 h at 353 K to remove ammonia and then refluxed under stirring for 18 h at 343 K. Then the gel was filtered and washed several times with distilled water at 343 K. The solids were eventually dried in an oven at 393 K for 72 h.

The Ni/Mg/Al contents in the coprecipitates were determined by X-ray fluorescence spectroscopy and atomic absorption spectroscopy. Their composition values are given in Table 1.

Sample calcination was carried out under a flow of air, in a programmed furnace. The

Table 1
Chemical composition of samples H1–H3

Sample	Chemical analysis					Total weight loss (%) on thermal decomposition	Sample formulae
	Ni (%)	Mg (%)	Al (%)	C (%)	N (%)		
H1	39.05	—	6.70	1.17	3.29	34.5	$Ni_{2.82}Al_1(OH)_{7.64}(CO_3)_{0.09}NO_3)_{0.82} \times 2.46H_2O$
H2	27.67	3.33	8.89	1.71	3.07	38.9	$Mg_{0.42}Ni_{1.43}Al_1(OH)_{5.7}(CO_3)_{0.19}(NO_3)_{0.62} \times 2.5H_2O$
H3	24.51	10.31	7.42	1.65	—	32.3	$Mg_{1.56}Ni_{1.52}Al_1(OH)_{8.16}(CO_3)_{0.5} \times 2.15H_2O$

temperature was increased from room temperature to 623, 773 and 973 K, at a rate of 2 K/min, the latter temperatures isothermally maintained for 2 h.

Each sample was then reduced in a nitrogen stream with a 10 vol% of hydrogen at 723 K (sample H3 was also reduced at 923 K). The reduction degree of the samples was determined by hydrogen consumption.

2.2. BET areas

BET surface areas were calculated from the nitrogen adsorption isotherms at 77 K using a Micromeritics ASAP 2000 surface analyzer, and a value of 0.164 nm^2 for the cross section of the nitrogen molecule.

2.3. X-ray diffraction (XRD)

The XRD patterns were recorded on a CGR Theta 60 Instrument using monochromatized Cu $K_{\alpha 1}$ radiation. Structural evolutions with temperature in air and under reducing atmosphere were studied in-situ with a high temperature XRD attachment (Barret-Gerard system) adapted on a CGR Theta 60 goniometer.

X-ray line broadening calculation of particle size for the oxidic and reduced phases was carried out using the Scherrer equation, applied to the more intense diffraction lines.

2.4. Temperature-programmed reduction (TPR) and thermogravimetric analysis (TGA)

These techniques were carried out in a Perkin-Elmer TGA 7 microbalance with and accuracy of 1 μg and equipped with a 272–1273 K programmable temperature furnace. TPR experiments were performed with H_2/Ar mixture (H_2/Ar, 5/95) from room temperature up to 973 K at 5 K/min. Thermogravimetric analysis (TGA) were carried out with the microbalance operating in a flow of dry helium (80 ml/min) at a heating rate of 2 K/min. Thermal decompositions and TPR of the samples were also followed by mass spectrometry using a Fisons Mass Spectrometer QTMD equipped with a 273–1273 K programmable temperature furnace.

2.5. Electron microscopy (TEM, FE-SEM)

Microstructural characterization of the material was performed by field emission scanning electron microscopy on a Leica Stereoscan 360 FE microscope and by transmission electron microscopy on a JEOL 200CX instrument. Thin foils of the solids were obtained by ultramicrotome using a diamond knife on grains embedded in an epoxy resin. In order to obtain both better resolutions and contrasts the micrographs (FE-SEM) were obtained at lower acceleration voltages.

2.6. Catalytic activity determination

A typical catalytic test was performed in a microflow reactor operated at atmospheric pressure. Prior to any measurement, 40 mg of sample was activated in situ. The sample was first calcined under O_2/N_2 mixture (20/80, vol/vol) from room temperature up to 623, 773 or 973 K at a rate of 2 K/min. After that, the sample was reduced at 723 K under a diluted hydrogen flow (H_2/N_2; 10/90, vol/vol). The reaction temperature ranged from 343 to 453 K.

Acetonitrile was fed by means of a positive displacement pump, and then diluted with hydrogen in a mixing chamber to obtain different acetonitrile/H_2 molar ratios. The reaction mixture was then passed through the catalyst and the effluent was analyzed by sampling on line to a gas chromatograph (Perkin Elmer) equipped with a capillary column and a flame ionization detector.

The products were identified by GC-MS coupling. All connecting lines, commutation and sampling valves were placed in a hot box heated at 373 K in order to prevent any condensation.

The conversion is defined by the following relation:

$$\text{acetonitrile conversion (mol\%)} = 100 \times (\text{acetonitrile}_{in} - \text{acetonitrile}_{out}) / \text{acetonitrile}_{in}$$

The selectivities have been calculated from peak areas taking into account the different sensitivity factors in the flame ionization detector and were defined as follows:

$$\text{Selectivity}_i\ \text{(mol\%)} = 100 \times (\text{corrected area})_i / (\text{sum of all corrected areas})$$

2.7. Adsorption heats and temperature programmed desorption (TPD)

The ethylamine adsorption heats were determined with a Setaram microcalorimeter DSC-111. The flowing gas passes through the catalytic bed, which is placed in the calorimetric cell. The sample was first activated as has been previously described for the catalytic test. Then, after outgassing under flowing He at 723 K, the sample was cooled to room temperature. Finally, the temperature was fixed to 313 ± 0.01 K, where micropulses of the probe molecules were fed onto the catalyst.

The thermal event in the calorimetric cell was then recorded as a function of the adsorbate uptake, which was monitored by a catharometer.

After the reactant adsorption, the temperature programmed desorption (TPD) of the adsorbate was performed under ultra pure argon. The temperature was raised from 313 to 800 K at 10 K/min. The composition of evolved gas was followed by a catharometer.

3. Results and discussion

3.1. BET areas

The BET areas of the precursors calcined at different temperatures and summarized in Table 2, show that the specific surface area values are ranging from 15–30 m^2/g for the non-calcined samples up to 200–240 m^2/g for the calcined ones. This increase of specific surface area takes place with a decrease of the average pore radius (19 to 5 nm). It is important to remark that the specific area and the stability in the temperature range from 623 to 973 K increase with the Mg content of the samples. The adsorption isotherms are of type II according to the IUPAC classification of adsorption isotherms. The calcined samples are mesoporous materials with average pore diameter around 5 nm.

Table 2
Pore volume and average pore radius from physical adsorption measurements

Sample	Pore volume (ml/g)	Average radius (nm)	BET surface area (m^2/g)
H1 (nc)	0.075	19.51	15.47
H1 (623 K)	0.236	4.89	192.75
H1 (773 K)	0.243	5.69	171.04
H1 (973 K)	0.242	6.32	153.55
H2 (nc)	0.109	17.19	25.48
H2 (623 K)	0.299	5.69	210.22
H2 (773 K)	0.354	6.66	212.26
H2 (973 K)	0.356	7.04	202.04
H3 (nc)	0.109	16.59	31.40
H3 (623 K)	0.340	5.10	220.38
H3 (773 K)	0.365	5.25	240.32
H3 (973 K)	0.257	6.35	174.80

(nc) = non-calcined
(623 K) = calcined at 623 K.

3.2. X-ray diffraction

The X-ray diffraction patterns of the non-calcined samples show the characteristic lamellar structure as reported in Table 3. The values of c' (calculated from the first basal reflection d_{003}) depicted in this table show that the sample H3, which has only carbonate ions in the interlayer (Table 1), exhibits the lowest values of c' (7.46 Å). This latter is very similar to the expected values from hydrotalcite-type compounds [27]. However, samples H1 and H2, also containing nitrate ions in the interlayer, have a

Table 3
X-ray diffraction of the non-calcined H1, H2, and H3 samples

	d (Å)	I/I_i	L (Å)
H1	8.10	100	111
	4.05	23	
	2.52	4	
	2.42	4	
	1.52	6	
H2	8.83	100	84
	4.39	39	
	2.57	10	
	1.50	4	
H3	7.46	100	167
	3.77	42	
	2.55	33	
	1.51	21	
	1.48	15	

L = particle size calculated using the Scherrer equation.

Table 4
X-ray diffraction of the sample H2 at different calcination temperatures

	d (Å)	I/I_i	L (Å)
H2 (non-calcined)	8.83	100	84
	4.39	39	
	2.57	10	
	1.50	4	
H2 (623 K)	2.44	47	
	2.07	100	65
	1.47	36	
H2 (773 K)	2.53	5	
	2.44	47	
	2.07	100	75
	1.47	36	
H2 (973 K)	2.53	10	
	2.43	40	
	2.07	100	85
	1.47	36	

L = particle size calculated using the Scherrer equation.

much larger interlayer spacing than H3. This behavior is in agreement with other behavior from the literature [28].

The XRD patterns of the sample H2 calcined at different temperatures are shown in Table 4. The crystallographic transition from lamellar to the mixed oxide structures can be observed from 623 K detecting mainly the NiO phase. It must be noted in the XRD pattern of H2 the appearance, with the rise of calcination temperature, of a weak reflection at $d = 2.53$ Å not belonging to the mixed oxide structure and which could be assigned to a non-stoichiometric magnesium aluminate spinel-type phase [29–31].

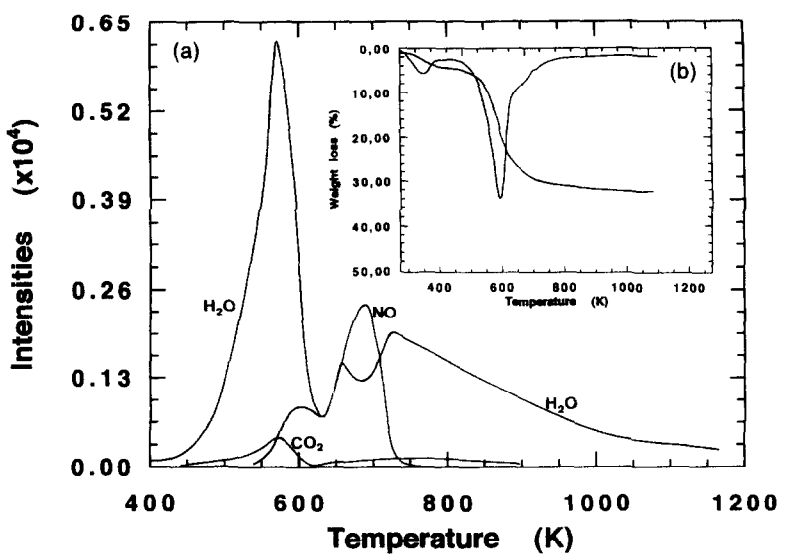

Fig. 1. (a) Thermal decomposition versus temperature performed in an ultra-high vacuum mass spectrometer. (b, inset) Weight decrease versus time for the thermal decomposition of sample H1 at a temperature between 323 and 1123 K, and a heating rate of 2 K/min.

The average size of the NiO particles calculated using the Scherrer equation is in every case in the range of 65–85 Å.

3.3. Temperature-programmed reduction (TPR) and thermogravimetric analysis (TGA)

Fig. 1a, b shows the thermogravimetric analysis of the sample H1 detecting the gases evolved during heat treatment by mass spectrometry (a) and also the weight loss during the same treatment (b). Two weight losses characteristic of the hydrotalcite-type compounds have been observed. The three samples show a similar behavior. The total weight loss is around 34–38% (Table 1). The main species detected by mass spectrometry during the decomposition process are: H_2O, CO_2 and NO for the samples H1 and H2, and only water and CO_2 for the sample H3.

The first weight loss in the TG analysis is due to the departure of weakly bonded water, which is probably the hydration water located in the interlayer space. A second step of water release is performed between 540 and 700 K accompanied by the departure of CO_2 and one part of NO. A new emission of NO altogether with H_2O is produced at temperatures between 700 and 800 K. These latter processes convey the decomposition of the hydrotalcite-type structure. After that, a constant release of water is performed up to a temperature of 1000 K. This water is probably obtained from the dehydroxylation of the Al_2O_3 phase. It can be deduced from this analysis that the nitrate ion is more strongly bonded than the carbonate one.

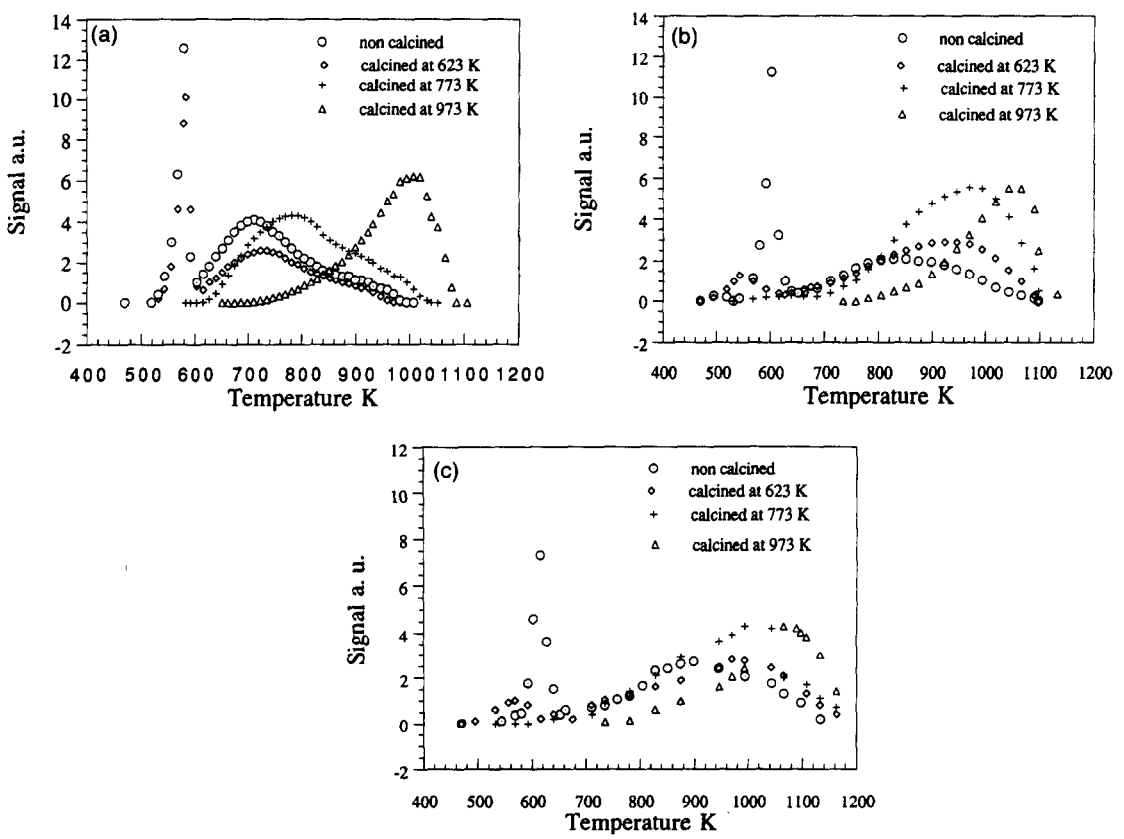

Fig. 2. Temperature programmed reduction for the samples H1 (a), H2 (b) and H3 (c) calcined at different temperatures.

Table 5
Some characterization parameters obtained from the LDH samples

Sample	Calcination temperatures (K)	Reduction degree	L [a] (Å)	Metal area [b] (m^2/g)	Activation energy (kJ/mol)
H1	623	0.55	89	13	75
	773	0.28			
	973	0.07			
H2	623	0.30	74	8	68
	773	0.11			
	973	0.03			
H3	623	0.05			
	773	–			
	973	–			

[a] Calculated using the Scherrer equation.[b] Calculated by H_2 chemisorption at 298 K.

The TPR curves of the non-calcined and calcined three samples at 623, 773 and 973 K are depicted in Fig. 2a, b, c. Two peaks are observed when the sample H1 is non-calcined or calcined at 623 K. In turn, practically only one peak can be observed for the samples H1 and H3 calcined at 623 K. It means that reduction proceeds with more difficulty both when the amount of Mg or/and Al in the layers of the LDH increases and the calcination temperature rises, as can also be seen in Table 5. However the apparent activation energy for the reduction process, the Ni particle size and the metal area of the samples H1 and H2, show similar values (Table 5).

Fig. 3. Scanning electron micrographs from the non-calcined sample H1 (a) and calcined at 973 K (b).

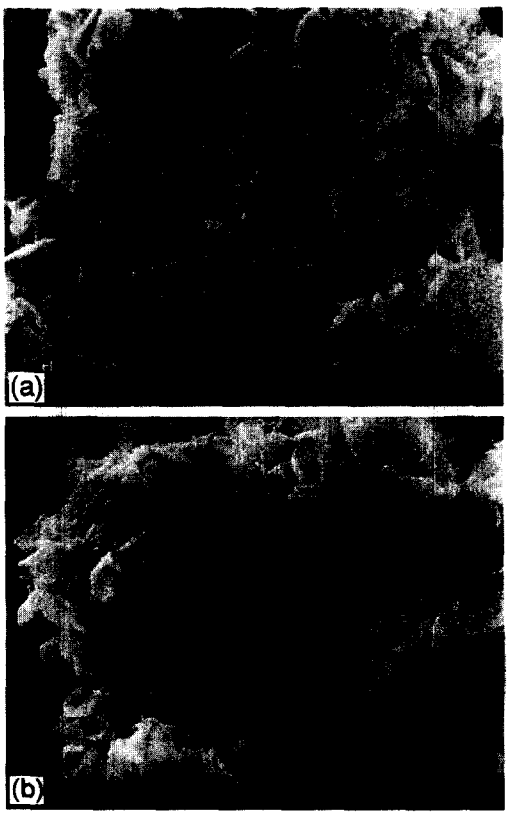

Fig. 4. Scanning electron micrographs from the samples H1 (a) and H2 (b) calcined at 623 K and after reduction at 623 K.

At higher calcination temperatures only one broad reduction peak is observed for the three samples. The first sharp reduction peak at about 573–623 K is unchanged by the calcination at 623 K for the sample H1 but is shifted to lower temperatures in H2. This first peak can be assigned to the reduction process of the Ni^{2+} still belonging to the layer structure of the LDH or to the NiO type phase obtained during the calcination process. The second broad reduction peak, which is shifted toward higher tempera-

tures when the calcination temperature increases or when the amount of Mg is higher, can be attributed to the reduction of a Ni–Al or Ni–Mg–Al spinel phase [32–35]. If higher calcination temperatures are used the reduction process can only be achieved at temperatures near 1000 K, obtaining lower reduction degrees under those conditions (Table 5).

3.4. Electron microscopy (TEM, FE-SEM)

Stereographic pictures of calcined at 973 K and non-calcined sample H1 are shown in Fig. 3a, b. The morphologies of sample H1 and the other samples, are characteristic of hydrotalcite-type materials [35,36] with a platelet thickness ranging from 10 to 15 nm. After calcination up to 973 K, the general morphology is preserved but with a nodular appearance. These nodules of about 10 nm in size are probably the NiO particles revealed by XRD.

Micrographs of samples H1 and H2 calcined at 623 K and reduced at 623 K are shown in Fig. 4a, b (FE-SEM) and Fig. 5a, b (TEM). The FE-SEM results show the presence of a nodular appearance for the sample H1, probably due to the reduced nickel obtained during the reduction process in complete agreement with the former XRD data and TPR results. The morphology of this sample after the reduction process is also characteristic of a hydrotalcite-type material. However, this nodular appearance has not been observed by FE-SEM for the samples H2, probably due to a lower reduction degree. Furthermore, using the TEM technique, metal Ni particles have been detected for the two samples, as shown in Fig. 5a, b. Although, the sample H2, which contains Mg, shows a better dispersion for NiO and Ni than sample H1, the metal particle sizes detected by TEM are similar for the two samples ranging from 5 up to 15 nm.

It can be stated, from FE-SEM, that the physical appearance of the materials is the same at all stages, when precipitated, calcined and

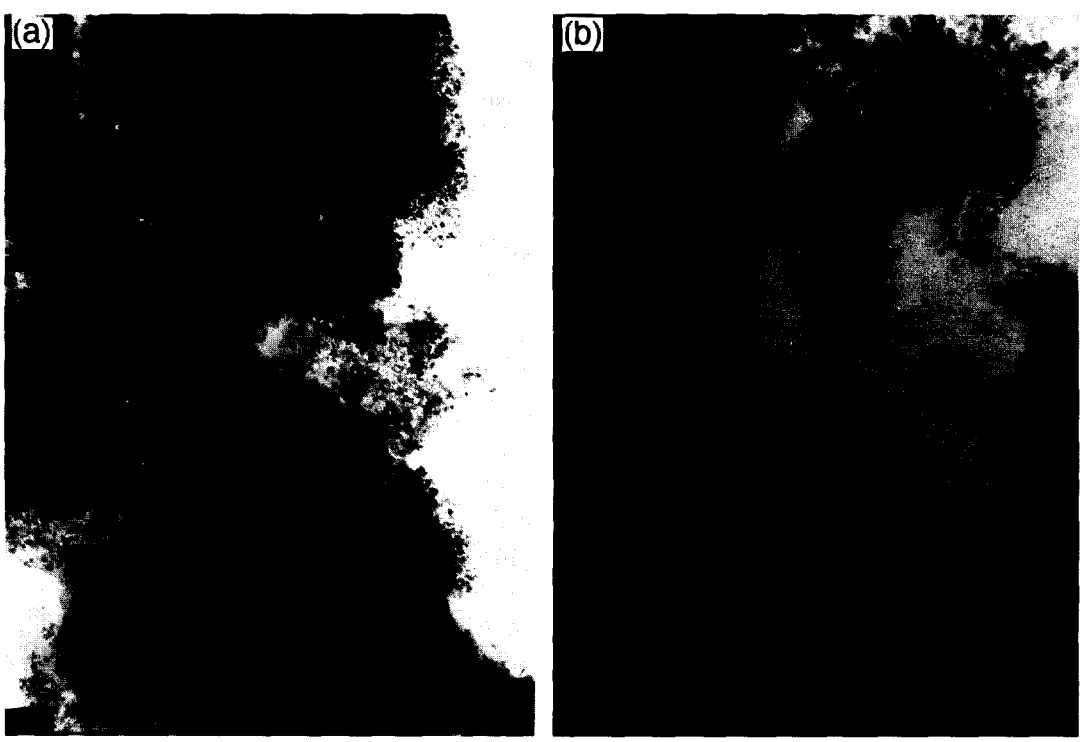

Fig. 5. Transmission electron micrographs from the samples H1 (a) and H2 (b) calcined at 623 K and after reduction at 623 K.

reduced. In summary, the physical skeleton of the calcined samples before and after reduction is probably provided by an alumina-rich phase [37].

3.5. Catalytic results

In a set of experiments, the catalysts were tested by temperature programmed reaction from 353 to 453 K by steps of 10 K and plateaux of 2 h in which the following reactant pressures were chosen: $p(H_2) = 88$ kPa and P(acetonitrile) = 13 kPa. Only the samples H1 and H2 calcined at lower temperatures (623 K) showed higher

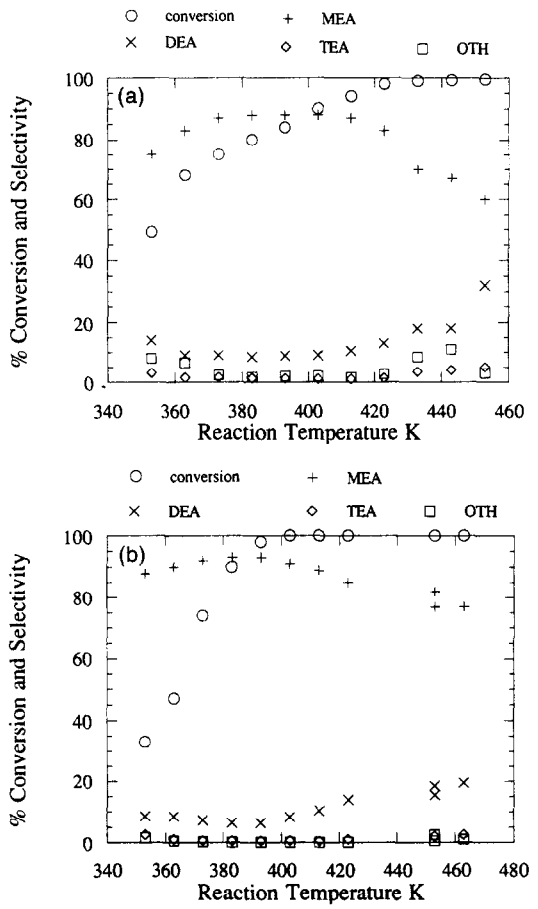

Fig. 6. Conversion and selectivity for acetonitrile hydrogenation obtained from the H1 (a) and H2 (b) samples calcined at 623 K and reduced at 723 K. Symbol OTH = diethylimine at lower reaction temperatures and ethane and methane at higher reaction temperatures.

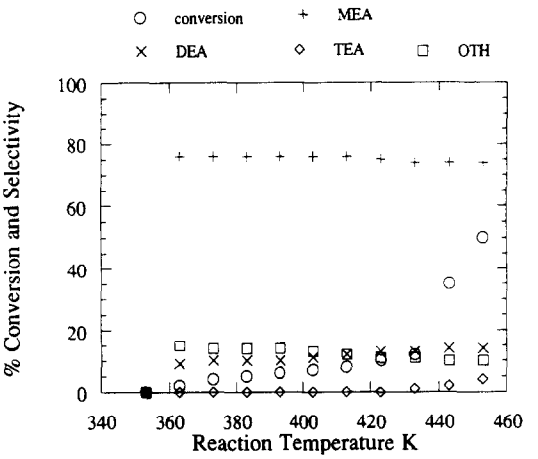

Fig. 7. Conversion and selectivity for acetonitrile hydrogenation obtained from H3 sample calcined at 623 K and reduced at 923 K. Symbol OTH = in Fig. 6.

catalytic activities. The plots of acetonitrile conversion, MEA (monoethylamine), DEA (diethylamine) and TEA (triethylamine) selectivities are shown in Fig. 6a, b. The sample H3 was inactive due to its practically null reduction degree. From these results, we can state that the sample H2 shows higher activity and selectivity to MEA than the H1 one. Also, the activity increases with the temperature reaction for both catalysts. Whatever the catalyst, the MEA selectivity reaches a maximum value in respect to the reaction temperature. Consequently, when replacing part of Ni by Mg as divalent cation an increase of both reactivity and MEA selectivity at low Mg content has been observed.

The by-products are mainly DEI (diethylimine) at low temperature and conversion and DEA and TEA at high temperature and conversion. Also traces of methane and ethane have been detected.

The metal surface area has been calculated for the two catalysts by H_2 chemisorption obtaining 13 m^2/g and 8 m^2/g for H1 and H2 samples, respectively (Table 5), whereas the conversions of the latter two catalysts for the acetonitrile hydrogenation at 393 K have been 60 and 100%, respectively. It seems, that the metal area value is not too relevant in respect to the catalytic activity.

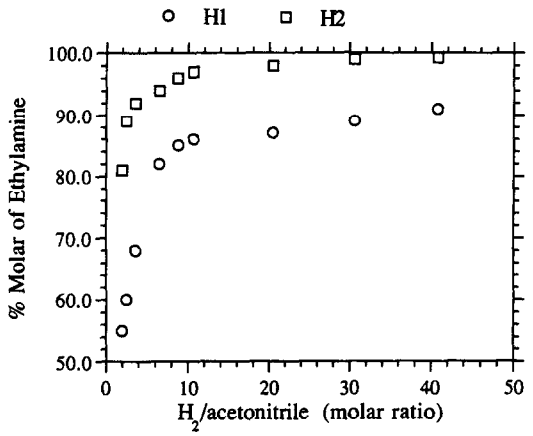

Fig. 8. Selectivities to ethylamine from catalysts H1 and H2 at a reaction temperature of 373 K by changing the H2/acetonitrile ratios.

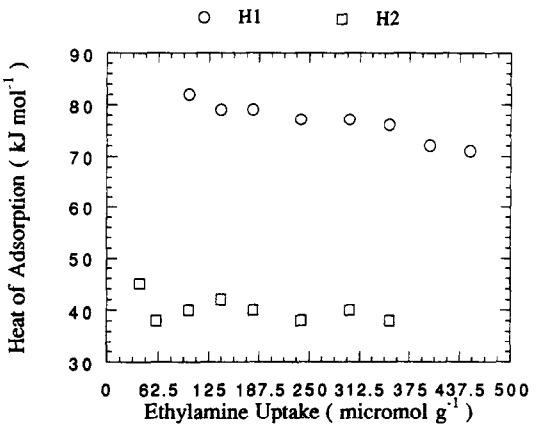

Fig. 9. Adsorption heats of ethylamine against the cumulative amount adsorbed on H1 and H2 catalysts.

Another experiment has been performed using the sample H3 reduced at 923 K, which shows a metal area value of 9 m^2/g. The results are depicted in Fig. 7. This catalyst shows lower activity and selectivity in relation with MEA. Consequently, the catalytic behavior is by far influenced by the chemical composition of the catalyst in agreement with the literature data [14].

The selectivity to MEA for the catalysts H1 and H2 at a reaction temperature of 373 K by changing the H_2/acetonitrile ratios has also been performed. The results are shown in Fig. 8. The selectivity to MEA increases for both catalysts with the rise of H_2/acetonitrile ratios, obtaining selectivities to MEA higher than 91 and 99%, respectively. This fact can be explained taking into account the nitrile hydrogenation reaction mechanism [1,14]. Higher hydrogen pressures bring about an increase in the hydrogenation reaction rates resulting into a decrease in the condensation reaction which conveys the formation of secondary and tertiary amines.

3.6. Adsorption heats and temperature programmed desorption (TPD)

To study the different H1 and H2 catalytic behavior and check any differences in the acido-basicity of the samples, a microcalorimetric study of MEA adsorption and its temperature programmed desorption was carried out. Fig. 9 shows plots of the differential adsorption heat versus the cumulative amount of MEA. These results show that MEA adsorption is more energetic by 40 kJ/mol in the H1 compared to the H2 sample. This fact results in a more acidic behavior of the catalyst H1 than the H2 one, the latter being in agreement with the TPD results of MEA (Fig. 10). There is only one desorption peak occurring at low temperature ($\approx$ 450 K) in the H2 sample, whereas two additional desorption peaks at around 550 and 780 K occur in the H1 sample. This lower interaction between the MEA and the catalytic surface for the sample

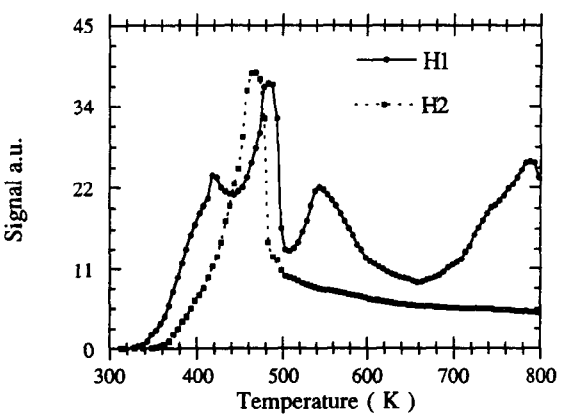

Fig. 10. Temperature programmed desorption profiles for ethylamine on H1 and H2 catalysts.

H2 could explain the higher selectivity to primary amine compared to the H1 catalyst.

4. Conclusions

The preparation and characterization of three hydrotalcite-type compounds and their catalytic behavior on the acetonitrile hydrogenation reaction in gas phase have been performed.

The specific surface areas in the range of 15–30 m^2/g for the non-calcined samples increase up to a maximum value of 190–240 m^2/g at 623 K with no micropores present. Surface areas also increase with the increase of magnesium content.

Nitrate and carbonate are the compensating anions for the H1 and H2 samples. However, sample H3 shows only carbonate as compensating anion.

All samples show the characteristic XRD patterns of hydrotalcite-type phases. The crystallographic transition from lamellar to the mixed oxide structures can be observed from 623 K. H1 and H2 both with interlayer nitrates show interlayer distances larger than in H3.

TPR experiments evidenced that the reducibility of the nickel oxide particles decrease with either the increase of calcination temperature or the increasing Mg and Al contents of the samples. Then the ease of reduction was in the order, H1 > H2 > H3.

Transmission and scanning electron microscopy show a higher metallic dispersion of reduced nickel with the increase of magnesium content.

The catalytic results show that when replacing part of the Ni by Mg as divalent cation, there is an increase of both reactivity and selectivity to MEA. However, when the amount of Mg is higher (sample H3) a decrease on both reactivity and selectivity is conveyed. On the other hand, it has been observed for all samples, that a H2/acetonitrile ratio rise produces higher selectivities to MEA.

The higher selectivity to MEA observed from sample H2 with respect to H1 can be explained by a lower acidic behavior of the catalyst H2 than the H1 one.

To sum up, hydrotalcite-type anionic clays can be useful as precursors of catalysts for the acetonitrile hydrogenation reaction. The addition of magnesium produces modifications both on the activity and the selectivity of the catalysts, obtaining higher selectivities towards primary amines. Furthermore, the production of primary amines is usually accomplished under a high ammonia pressure to suppress the condensation reactions yielding secondary and tertiary amines, hence, the catalysts obtained from basic anionic clays might have a potential interest for the manufacture of primary amines.

Acknowledgements

We gratefully acknowledge the support of this work by the Comisión Interministerial de Ciencia y Tecnología (project PR95-094).

References

[1] K. Weisssermel and H.J. Arpe, Industrial Organic Chemistry (Verlag Chemie, Berlin, 1978).
[2] A.Y. Lazaris, E.N. Zil'berman, E.V. Lunicheva and A.M. Vedin, Zh. Prikl. Chim. 38 (1965) 1097.
[3] F. Medina, P. Salagre, J.E. Sueiras and J.L.G. Fierro, J. Mol. Catal. 68 (1991) L17.
[4] H. Greenfield, Ind. Eng. Chem. Prod. Res. Dev. 6 (1967) 142.
[5] J. Pasec, N. Kostova and B. Dvorak, Collect. Czech. Chem. Commun. 46 (1981) 1011.
[6] J. Bolle, Fr. Pat., 2063378 (1971).
[7] K. Kioki, K. Hirokawa, Y. Kuka and A. Shimade, Jpn. Kokai Tokkyo Koho, 7547909 (1975).
[8] W. Jerzykiewicz, Z. Krasnodebski and G. Bekierz, Pol. Pat., 115999 (1983).
[9] Ch.E. Kuthens and L.M. Lanier, U.S. Pat., 4429159 (1984).
[10] R. Uehara, T. Horri, T. Imai, Y. Tomita and K. Yamano, Jpn. Kokai Tokkyo Koho, 7678795 (1976).
[11] F. Mares, J.E. Galle, S.E. Diamond and F.J. Regina, J. Catal. 112 (1988) 145.
[12] F. Medina, P. Salagre, J.E. Sueiras and J.L.G. Fierro, J. Mol. Catal. 61 (1990) 197.
[13] R.L. Augustine, Catal. Rev. 13 (1976) 285.
[14] M.J.F.M. Verhaak, A.J. Van Dillen and J.W. Geus, Catal. Lett. 26 (1994) 37.

[15] F. Medina, P. Salagre, J.E. Sueiras and J.L.G. Fierro, Appl. Catal. A: General 92 (1992) 131.
[16] P. Courty, D. Durand, E. Freund and A. Surgier, J. Mol. Catal. 17 (1982) 241.
[17] Pl. Gherardi, O. Ruggeri, F. Trigirò, A. Vaccari, G. Del Piero, G. Manara and B. Notari, in: G. Poncelet, P. Orange and P.A. Jacobs (Editors), Preparation of Catalysts III, Studies in Surface Science and Catalysis , Vol. 16 (Elsevier, Amsterdam, 1983) p. 723.
[18] G. Fornasari, S. Gusi, F. Trifirò and A. Vaccari, Ind. Eng. Chem. Res. 29 (1987) 1500.
[19] E.C. Kruissink, L.L. Van Reijen and R.R.H. Ross, J. Chem. Soc. Faraday Trans. I 77 (1981) 649.
[20] L.E. Alzamora, J.R.H. Ross, E.C. Kruissink and L.L. Van Reijen, J. Chem. Soc. Faraday Trans. I 77 (1981) 665.
[21] E.B.M. Doesburg, P.H.M. De Korte, H. Shaper and L.L. Van Reijen, Appl. Catal. 11 (1984) 155.
[22] H.G.J. Lansink Rotgerink, H. Bosch, J.G. Van Ommen and J.R.H. Ross, Appl. Catal. 27 (1986) 41.
[23] A. Corma, V. Formés and F. Rey, J. Catal. 148 (1994) 205.
[24] S. Miyata, Clays Clay Miner. 28 (1980) 50.
[25] S. Miyata, T. Kumura, H. Hattori and K. Tanabe, J. Chem. Soc. Jpn. 92 (1971) 514.
[26] T. Reichle, S.Y. Kangand D.S. Everhardt, J. Catal. 101 (1986) 352.
[27] D.L. Bish and G.W. Brindley, Am. Mineral. 62 (1977) 458.
[28] S. Miyata, Clays Clay Miner. 31 (1983) 305.
[29] J. Hu, J.A. Schwarz and Y.J. Huang, Appl. Catal. 51 (1989) 223.
[30] B. Rebours, J.B. d'Espinose de la Caillerie and O. Clause, J. Am. Chem. Soc. 116 (1994) 1707.
[31] A. Vaccari and M. Gazzano, in: B. Delmon and J.F. Yates (Editors), Preparation of Catalysts VI, Studies in Surface Science and Catalysis, Vol. 91 (Elsevier, Amsterdam, 1995) p. 893.
[32] S.K. Shaikhutdinov, L.B. Avdeeva, O.V. Goncharova, D.I. Kochubey, D.I., Novgorodov and L.M. Plyasova, Appl. Catal. A 126 (1995) 125–139.
[33] J.M. Rynkowski, T. Paryjczak and M. Lenik, Appl. Catal. 106 (1993) 73–82.
[34] P.H. Bolt, S.F. Lobner, J.W. Geus and F.H.P.M. Habraken, Appl. Surf. Sci. 89 (1995) 339–349.
[35] P. Courty and D. Durand, in: B. Delmon et al. (Editors), Preparation of Catalysts IV (Elsevier, Amsterdam, 1987) p. 739.
[36] F. Thevenot, F. Szymanski and P. Chaumette, Clays Clay Miner. 37 (1989) 396.
[37] E.B.M. Doesburg, G. Hakvort, H. Shaper and L.L. Van Reijan, Appl. Catal. 7 (1983) 85.